



ORIGINAL ARTICLE

Degradation of parathion methyl by reactive sorption on the cerium oxide surface: The effect of solvent on the degradation efficiency



Pavel Janoš^{a,*}, Jakub Ederer^a, Martin Štastný^b, Jakub Tolasz^{a,b}, Jiří Henych^{a,b}

^a Faculty of Environment, University of Jan Evangelista Purkyně, Pasturova 3632/15, 400 96 Ústí nad Labem, Czech Republic

^b Institute of Inorganic Chemistry of the Czech Academy of Sciences, 250 68 Husinec-Řež, Czech Republic

Received 14 November 2021; accepted 22 March 2022

Available online 29 March 2022

KEYWORDS

Cerium oxide;
Toxic organophosphate
destruction;
Solvent effect;
Reaction mechanisms;
Nucleophilic substitution
S_N2

Abstract A simple and easily scalable “wet” procedure was used to prepare nanocrystalline cerium oxide capable of destroying the toxic organophosphate pesticide parathion methyl. The synthetic procedure consists of the direct precipitation of cerous salt with aqueous ammonia in the absence of CO₂. The prepared cerium oxide was able to decompose the organophosphate compounds both in nonpolar (e.g., heptane) and polar aprotic (e.g., acetonitrile) solvents. However, in solvents with hydrogen-bond donating ability, the –OH groups on the cerium oxide surface were solvated and inactivated. The preferential solvation model was used to express the experimental dependencies of the cerium oxide degradation efficiency on the composition of the water-acetonitrile mixture. In certain solvent systems, some empirical polarity scales, such as the alpha-scale or the Dimroth-Richardt parameter $E_T(30)$, may be correlated with the degradation efficiency of cerium oxide.

© 2022 The Authors. Published by Elsevier B.V. on behalf of King Saud University. This is an open access article under the CC BY license (<http://creativecommons.org/licenses/by/4.0/>).

1. Introduction

Nanostructured metal oxides with specific designs have been extensively used for the destruction of toxic chemicals since the pioneering works of Klabunde et al. (1996) at the turn of the century (Khaleel et al., 1999; Rajagopalan et al., 2002; Lucas et al., 2001). Magnesium

oxide and titanium dioxide are representatives of the first generation of so-called “reactive sorbents” that are able not only to accumulate toxic substances on their surfaces but can also to destroy them (at least partially) and convert them into less toxic residuals. The family of reactive sorbents was extended substantially by Štengl et al. (2016; Houšková et al., 2007; Štengl et al., 2012); who also introduced new environmentally friendly wet synthetic procedures for their preparation.

Nanostructured metal oxides are especially effective in the decomposition of toxic organophosphates, including organophosphate pesticides (Janoš et al., 2014), nerve-paralytic chemical warfare agents, some kinds of flame retardants (Janoš et al., 2014; Ederer et al., 2019) and other derivatives (triesters) of phosphoric or thiophosphoric acids. Denet et al. (2020) recently compared the decontamination activity of several metal oxides (MgO, TiO₂, CeO₂, ZnO and ZrO₂) against both chemical and biological agents. They also discussed the

* Corresponding author.

E-mail address: pavel.janos@ujep.cz (P. Janoš).

Peer review under responsibility of King Saud University.



Production and hosting by Elsevier

effects of various solvents on the chemical degradation efficiency of metal oxides and attempted to explain them using the concept of eluent strength, which is derived from liquid chromatography.

In our first study on the utilization of cerium oxide as a reactive sorbent (Janos et al., 2014); we showed that the degradation of toxic organophosphates may be performed effectively both in nonpolar solvents, such as heptane, and polar aprotic (and thus water-compatible) solvents such as acetonitrile. While the reactivity of reactive sorbents in aqueous media is crucial for typical environmental applications such as wastewater treatment, the utilization of organic solvents for the decontamination of military equipment or for the destruction of stockpiled toxic chemicals may be more advantageous. However, a detailed understanding of the solvent effects on heterogeneously catalysed liquid phase reactions is still lacking (Gould et al., 2020). Therefore, we examined the degradation of parathion methyl, a representative toxic organophosphate compound, in the presence of cerium oxide in various solvents and solvent mixtures with the goal of clarifying the reaction mechanism(s) more exactly. The preferential solvation model was used to evaluate the experimental dependencies and to identify the main forces driving parathion methyl degradation in acetonitrile–water mixed solvent.

2. Materials and methods

2.1. Materials and chemicals

Cerium nitrate, $\text{Ce}(\text{NO}_3)_3 \cdot 6\text{H}_2\text{O}$, was obtained from Sigma-Aldrich (Steinheim, Germany) as a reagent-grade chemical with 99.9% purity (trace metal basis). The organophosphate pesticide parathion methyl (PM) and its degradation product 4-nitrophenol (4-NP) were obtained from Sigma-Aldrich as chromatographic standards. Aqueous ammonia solution (25–29%), NH_4OH , was obtained from Penta (Czech Republic) with p.a. purity. HPLC-grade methanol and acetonitrile were used as mobile phase constituents in liquid chromatography. The various organic solvents used as reaction media in this study were of reagent-grade or HPLC-grade purity and were obtained from Sigma-Aldrich.

2.2. Synthesis of cerium oxide

Cerium oxide was prepared by the direct precipitation of the cerium nitrate solution with aqueous ammonia under ambient conditions using the procedure described in our previous papers (Janoš et al., 2019; Tolasz et al., 2020) with slight modifications. Briefly, one litre of the cerium nitrate solution (0.05 mol/L) was agitated in a beaker with a thermostat at $22 \pm 2^\circ\text{C}$ and purged with air that had been cleaned of carbon dioxide by passing it through KOH solution (40%). Concentrated aqueous ammonia was added in several portions until the pH reached ca. 10. Extensive agitation and purging with de-carbonated air continued until the colour of the precipitate changed to a pale yellow (typically for ca 2 h). The precipitate was washed with deionized water several times and air-dried at 60°C . The air-dried cerium oxide was stored in tightly closed PE bottles and used without any additional thermal treatment unless otherwise specified. The sample was denoted as LT- CeO_2 .

For comparison, another kind of cerium oxide was prepared by the conventional “precipitation/calcination” method (Ederer et al., 2021) from cerous(III) carbonate by annealing in an open crucible at 500°C for 2 h. The sample was denoted as HT- CeO_2 .

More detailed descriptions of the synthetic procedures can be found in the Supplementary data.

2.3. Methods of characterization

Diffraction patterns were collected with a Bruker D2 diffractometer equipped with a conventional X-ray tube (Cu $\text{K}\alpha$ radiation, 30 kV, 10 mA) and a LYNXEYE 1-dimensional detector. A primary divergence slit module width 0.6 mm, Soler Module 2.5, Airscatter screen module 2 mm, Ni- $\text{K}\beta$ filter 0.5 mm, in the 2θ range of 5° – 90° with step 0.00808° and a time per step of 1.0 s were used. The crystallite sizes were calculated from the broadening of the diffraction line using the Scherrer formula ($d = K \lambda / \beta \cos\theta$ where K is the shape factor, λ is the wavelength, θ is the diffraction angle and β is the diffraction line broadening (Johnson and Mooi, 1987; Janoš and Petrák, 1991), calculations were performed on the X’Pert HighScore Plus software. The crystalline structure, shape and size of nanoceria were inspected by high-resolution transmission electron microscopy (HRTEM) using a 200 kV TEM microscope (FEI Talos F200X). As a specimen support for TEM investigations, a microscopic copper grid covered by a thin, transparent, holey carbon film was used. Suspensions of all the samples were diluted, ultrasonicated for a few minutes and dropped onto the copper grids. The specific surface areas and porosities of the powder samples were measured using a Belsorp maxII instrument at liquid nitrogen temperature. The samples were degassed for 4 h at 120°C . The Brunauer–Emmett–Teller (BET) method was used for surface area calculation. The acid-base properties of the cerium oxide samples were examined by potentiometric titration using an automatic titrator controlled by a PC (794 Basic Titrimo, Metrohm, Switzerland) using the method described in our previous works (Ederer et al., 2021; Ederer et al., 2017).

2.4. Parathion-methyl degradation tests

The original procedure was derived from the military standard STANAG 4653 (Stanag, 2012), which is used to test chemical warfare agents. In principle, a toxic substance is mixed with a relatively high excess of the decontamination agent, and its conversion to the reaction product(s) is followed by a suitable analytical method. The modification of the testing procedure for organophosphate pesticides is described in detail in our previous paper (Janos et al., 2014); therefore, we summarize only briefly the main characteristics of the test: 50 mg of the sorbent (cerium oxide) was weighed into a series of glass vials, and 150 μL of the pesticide solution in heptane (6660 mg/L) was added (the ratio of 1 mg of pesticide to 50 mg of the sorbent was maintained). At predetermined time intervals ranging from 0.5 to 128 min, the reaction was terminated by the addition of 2 mL of 2-propanol, the sorbent was separated by centrifugation, and the supernatant was transferred into a volumetric flask. The sorbent was redispersed in methanol (4 mL) and centrifuged again; the extraction of the cerium oxide with methanol was repeated 3 times, and all the supernatants were combined in one volumetric flask, which was made up with mobile phase used for the subsequent determination of parathion methyl and 4-nitrophenol by HPLC.

2.4.1. Degradation tests in mixed solvents

In a typical arrangement, the stock solution of parathion methyl (5 g/L) in heptane was prepared. 50 mg of the sorbent was weighed into a glass vial and 0.5 mL of the pesticide solu-

tion in heptane was added, then 1 mL of other solvent was added (co-solvent). At a predetermined time, the reaction was terminated by the addition of 2-propanol, and the sorbent was extracted with methanol in a similar way as described above. The rate constant was calculated from the degree of conversion with the assumption that the reaction follows the pseudo-first order kinetics equation. In a similar way, the series of experiments was performed with the stock solution of parathion methyl in acetonitrile.

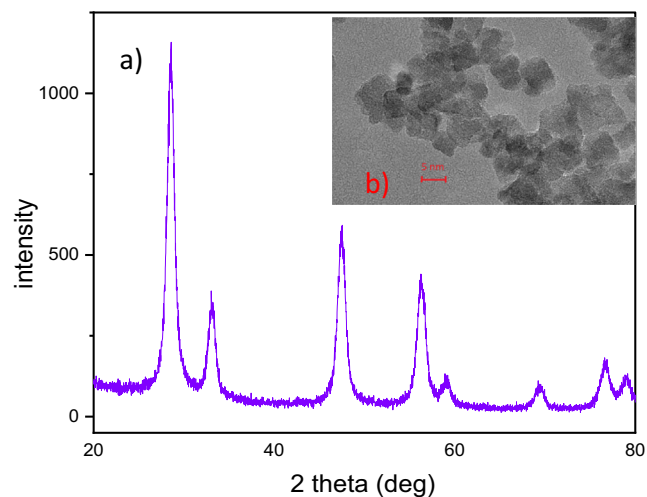


Fig. 1 (a) XRD pattern of air-dried cerium oxide LT-CeO₂; (b) HRTEM image of the same cerium oxide.

A slightly different procedure was used for measurements of kinetic dependencies: 100 mg of the sorbent was dispersed in 4.5 mL of the respective solvent, and the reaction was initiated by the addition of 0.5 mL of pesticide solution (5 g/L) in the same solvent. The reaction mixture was agitated with a small magnetic mixer. At predetermined time intervals, small amounts of the reaction mixture were taken and analysed immediately by HPLC.

3. Results and discussion

3.1. Characterization of cerium oxide

As seen from the X-ray diffraction pattern in Fig. 1, nanoparticulate cerium oxide with the well-developed fluorite-type crystalline structure can be prepared by the direct precipitation method under ambient conditions. The crystallite sizes estimated from the broadening of the diffraction peaks were 5.2 nm, which is in good agreement with microscopic (HRTEM) observations (see Fig. 1b, where poorly aggregated nanoparticles with cubic morphology can be distinguished). The number of surface hydroxyl groups was determined by acid-base titration. The value of 0.254 mmol/g is lower (but not dramatically – about 14%) than that determined for the cerium oxide annealed at 500 °C, whereas the pH values corresponding to the point of zero charge (PZC) were almost identical – 4.64 and 4.52 for LT-CeO₂ and HT-CeO₂, respectively. A comparison of the respective titration and TOTH curves is given in Fig. 2. Some other characteristics of the cerium oxides are given in Supplementary data.

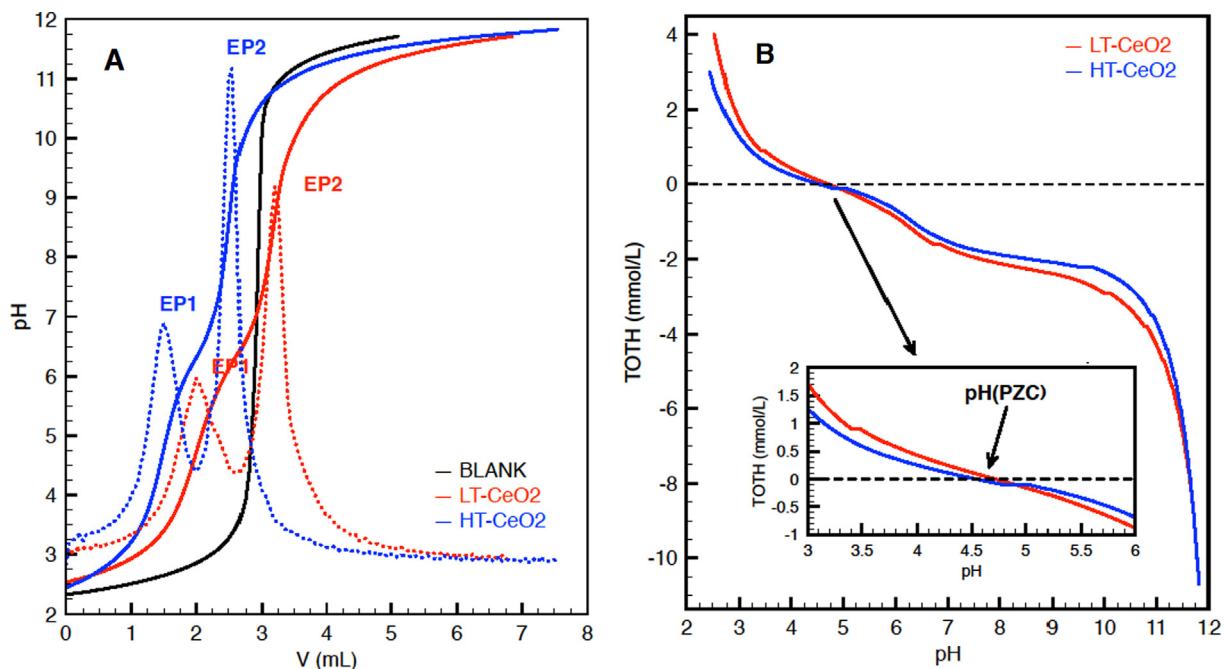


Fig. 2 (a) Titration curves (full lines) and their 1st derivations (dotted lines) of cerium oxides. EP1 and EP2 are the equivalent points corresponding to the base consumption; the content of the –OH groups was calculated from the difference between EP2 and EP1. (b) TOTH (total concentration of protons consumed in the titration process) curves derived from the titration curves. The inset plot details show the pH that corresponds to the point of zero charge (PZC).

3.2. Degradation of parathion methyl

The standardized testing procedure showed that cerium oxide synthesized at a low temperature destroys parathion methyl efficiently both in heptane (with a half-life of less than 5 min) and in acetonitrile (with a half-life of approximately 25 min) (see Fig. 3).

The degradation of parathion methyl in the presence of cerium oxide can be described as.



where A is parathion methyl, B is 4-nitrophenol and S are active sites on the cerium oxide surface. Assuming that $k_2 \gg k_1$, the conversion of parathion methyl to 4-nitrophenol may be described by the following kinetic equation:

$$-\frac{d[A]}{dt} = \frac{d[B]}{dt} = k_1[A][S] \quad (2)$$

with the integral form.

$$\ln \frac{[A]_t N_S w}{[A]_0 [S]_t} = k_1 ([A]_0 - w N_S) t$$

where $[A]_0$ and $[A]_t$ are the concentrations of parathion methyl at the beginning of the reaction and at time t , respectively, w is the mass concentration of cerium oxide in the reaction mixture, and N_S is the number of active sites in the cerium

oxide. Eq. (3) was used to fit the experimental data in Fig. 3; some model parameters obtained from the nonlinear fitting are listed in Table 1.

For comparison, the degradation of parathion methyl was performed in the presence of cerium oxide prepared by calcination at 500 °C from the carbonate precursor. It was found that both cerium oxides (the air-dried LT-CeO₂ and the high-temperature-treated HT-CeO₂) exhibited almost identical degradation efficiencies. To elucidate in more details this somewhat counterintuitive phenomenon, we performed additional experiments, in which we examined the degradation efficiency of the cerium oxides prepared by the calcination of the air-dried cerium oxide or cerium carbonate at different temperatures (for more detail see Supplementary data).

As can be seen from Fig. 4, the post-synthetic thermal treatment does not significantly affect the degradation efficiency of cerium oxide in a relatively broad temperature range from 200 to ca 600 °C. At higher temperatures (above 600 °C), however, the degradation efficiency of cerium oxide decreases steeply with increasing temperature. This behaviour is almost independent on the precursor used for the cerium oxide preparation. In the high-temperature region, the degradation efficiency may be clearly related to the number of hydroxyl groups on the cerium oxide surface, as shown in our previous work (Ederer et al., 2021).

At temperatures below 200 °C, on the other hand, the carbonate precursor is not destroyed, and therefore cerium

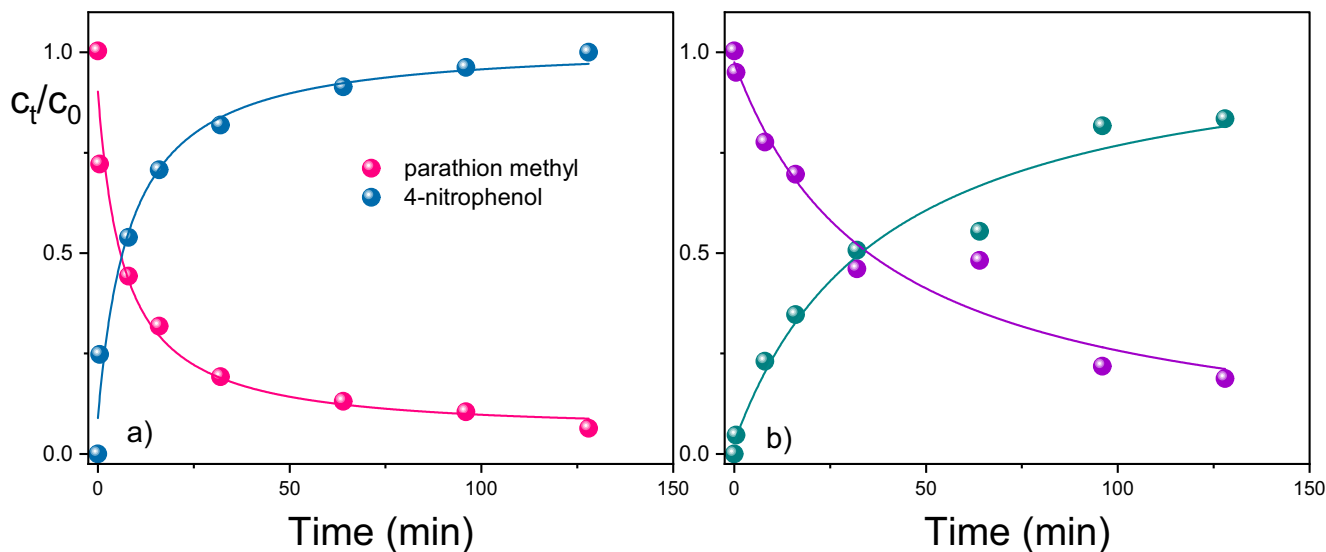


Fig. 3 Degradation of parathion methyl in n-heptane (a) and acetonitrile (b) in the presence of cerium oxide LT-CeO₂. Weight of sorbent = 0.05 g, 1 mg of parathion methyl dissolved in 0.15 mL of the respective solvent.

Table 1 Parameters of the kinetic dependencies of parathion methyl degradation.

Solvent	Parathion methyl destruction			4-nitrophenol creation		
	Rate constant (min ⁻¹ mol ⁻¹ L)	D ^a	R ²	Rate constant (min ⁻¹ mol ⁻¹ L)	D	R ²
n-heptane	0.185 (0.061) ^b	0.079 (0.068)	0.9717	0.137 (0.052)	0.054 (0.146)	0.9803
acetonitrile	0.029 (0.007)	-0.122 (0.159)	0.9926	0.026 (0.006)	-0.224 (0.154)	0.9959

^a Parameter D is related to the difference between the initial concentration of parathion methyl and the concentration of free active sites on cerium oxide at the beginning of the reaction.

^b The standard error is given in parentheses.

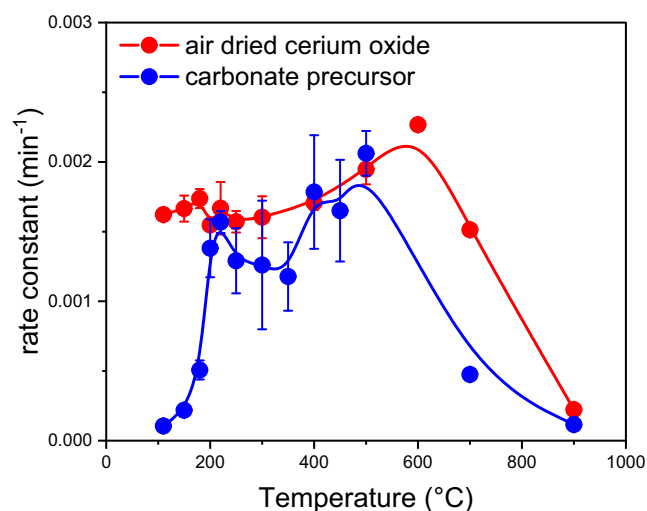


Fig. 4 Effect of the (additional) thermal treatment on the degradation efficiency of cerium oxides prepared from various precursors: Red points – samples prepared by the additional thermal treatment of the air-dried cerium oxide; blue points – samples prepared by the calcination of cerium carbonate.

oxide is not created. On the other hand, there is no such limitation for the cerium oxides prepared by the purely wet process (e.g., via precipitation of cerium hydroxides accompanied by the aqueous-phase oxidation with a subsequent dehydration and creation of the crystalline cerium oxide). Therefore, effective cerium oxides can be prepared even at temperatures close to zero (Janoš et al., 2019; Tolasz et al., 2020).

3.2.1. Proposed mechanisms of degradation of parathion methyl

The complex dependence of the degradation efficiency on the temperature of treatment suggests that several properties of cerium oxide affect its degradation efficiency. In general, morphology (including the crystal shapes) and surface chemistry (surface non-stoichiometry) govern the activity of the ceria nanoparticles, together with the crystalline structure that facilitates the mobility of oxygen vacancies and other defects on the cerium oxide surface (Seal et al., 2020).

In the phosphoester cleavage process, both cerium cations as well as surface hydroxyls are involved (Janos et al., 2014): the cerium cation coordinates the sulfur atom in the thiophosphate group of the parathion methyl, making the central phosphorus atom more susceptible to nucleophilic attack, whereas the hydroxyl groups on the cerium oxide surface serve as nucleophilic agents that attack the P atom of the thiophosphate group. Recently, Plakhova et al. (2019) and Artiglia et al. (2021) emphasized the role of surface hydroxyls not only for the biological activity of cerium oxide, but also for some industrial applications.

3.3. Degradation of parathion methyl in mixed solvents

In our previous paper (Janos et al., 2014); we demonstrated that the addition of even small amounts of polar solvent (typically water) may deteriorate the degradation efficiency of cerium oxide (see also Fig. 5). In the following series of experiments, we tested the degradation efficiency in mixed sol-

vents composed of heptane and another co-solvent (the ratio of heptane to co-solvent was 1:2) or acetonitrile with another co-solvent (the ratio was also 1:2). As shown in Fig. 6a, the systems with heptane as the main constituent are rather insensitive to changes in the composition of the reaction medium. Even the presence of polar solvents (acetonitrile) or higher alcohols does not disturb the degradation efficiency of cerium oxide. Mixed solvents with acetonitrile as the main constituent, however, are much more sensitive to the presence of co-solvents. The addition of polar and protic solvents significantly reduces the degradation ability of cerium oxide. This result is fully consistent with the presupposed reaction mechanism.

According to the theory of nucleophilic reactions, binuclear nucleophilic substitution reactions (S_N2) are suppressed in the presence of protic solvents (Hamlin et al., 2018), which are able to solvate the nucleophile via hydrogen bonding. The hydrogen bond donating (HBD) ability of solvents can be expressed, for example, with the aid of the α -scale introduced by Taft and Kamlet (1979). Marcus (Marcus, 1991) correlated the α -scale with other polarity scales, such as the $E_T(30)$, Z or A_N scales. We attempted to correlate the degradation efficiency of cerium oxide with the polarity parameters of the co-solvents used as reaction media for parathion methyl degradation (Fig. 6).

3.4. Study of parathion methyl degradation in an acetonitrile–water mixture

The following figure (Fig. 7) demonstrates that the addition of water (and, to a lesser degree, methanol) to acetonitrile dramatically deteriorates the degradation efficiency of cerium oxide as a result of the solvation of active sites mainly via hydrogen bonding and slows down the kinetics of the reaction.

To examine this effect in more detail, we measured the dependence of the degradation rate on the composition of the water-acetonitrile mixture over a wide concentration range. To express an effect of water addition on the reaction kinetics at least semi-quantitatively, a model that assumes the solvation of active sites in mixed solvents was proposed and used to fit the experimental data.

3.4.1. Solvation of active sites in the acetonitrile–water mixture

Water-acetonitrile mixtures are popular solvents in organic synthesis as well as in separation sciences because of the mutual miscibility of their components at any ratio and their solubilizing ability towards many organic and inorganic compounds. Despite the great number of studies devoted to this system, its properties are still not completely understood because of the inherently complex interactions of the components, which have quite different natures. Depending on the composition of the mixture (expressed in molar concentrations or mole fractions), various interactions (dipole–dipole interactions, hydrogen bonding) predominate in various concentration regions. It was deduced from X-ray diffraction and IR measurements (Takamuku et al., 1998) and from X-ray absorption spectrometry (Nagasaka et al., 2020) and computer simulations (Ahn and Lee, 2007) that acetonitrile, water and mixed clusters are present in the water-acetonitrile binary mixture. In a relatively large range of compositions (for $x_w = 0.25$ – 0.8 ; x_w – mole fraction of water), the presence of “microheterogeneities” is supposed.

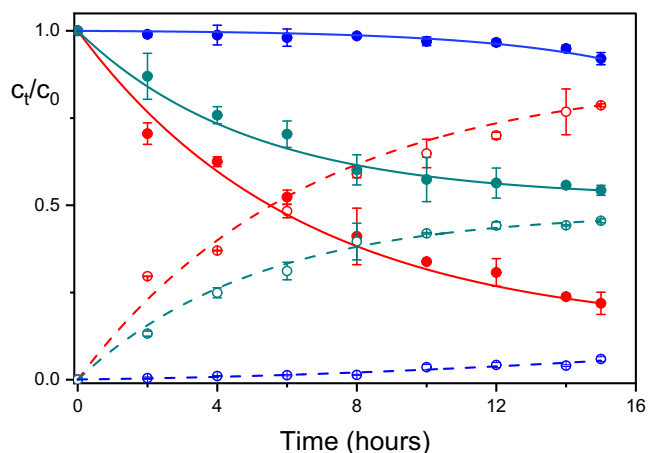
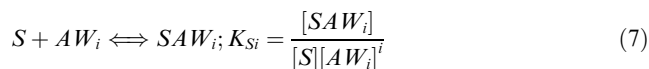
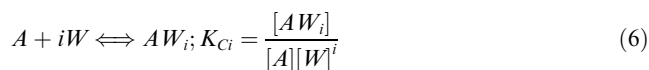
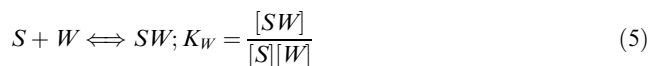


Fig. 5 Degradation of parathion methyl in the presence of cerium oxide in acetonitrile (red points and curves); in an acetonitrile-methanol mixture 50/50% v/v (green points and curves); and in an acetonitrile-water mixture 50/50% v/v (blue points and curves).

The creation of these microconstituents and their contribution to the solvation of the site on the cerium oxide surface may be described as follows:



where Eqs. (1) and (2) describe the solvation of the active site S with the molecules of acetonitrile and water, respectively, Eq. (3) describes the creation of the acetonitrile-water clusters, and Eq. (4) describes the solvation of the active site with these clusters.

It holds for the active site:

$$c_S = [S] + [SA] + [SW] + [SAW] + \dots + [SAW_i] =$$

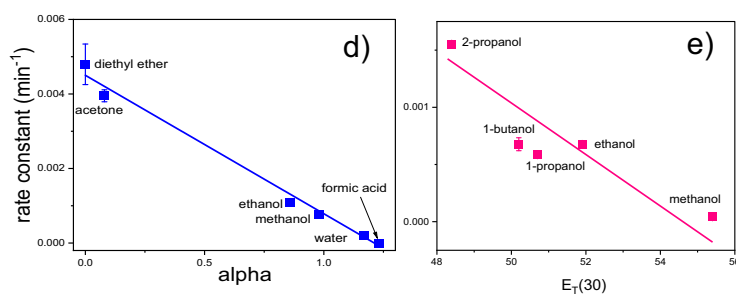
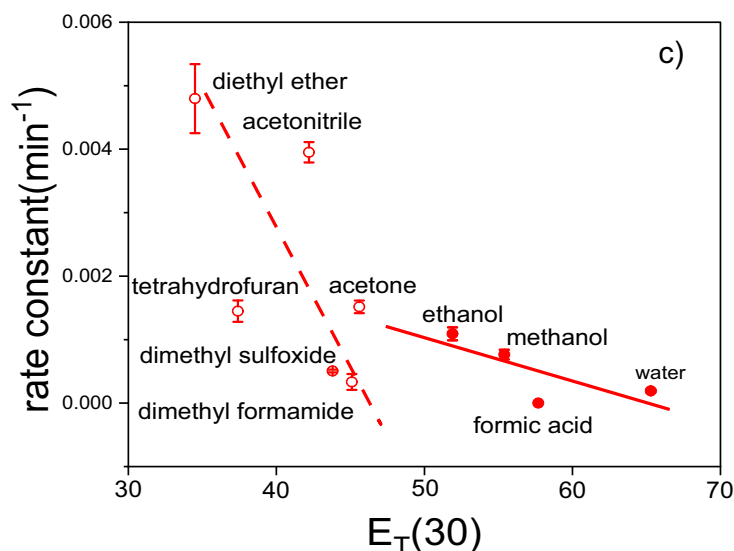
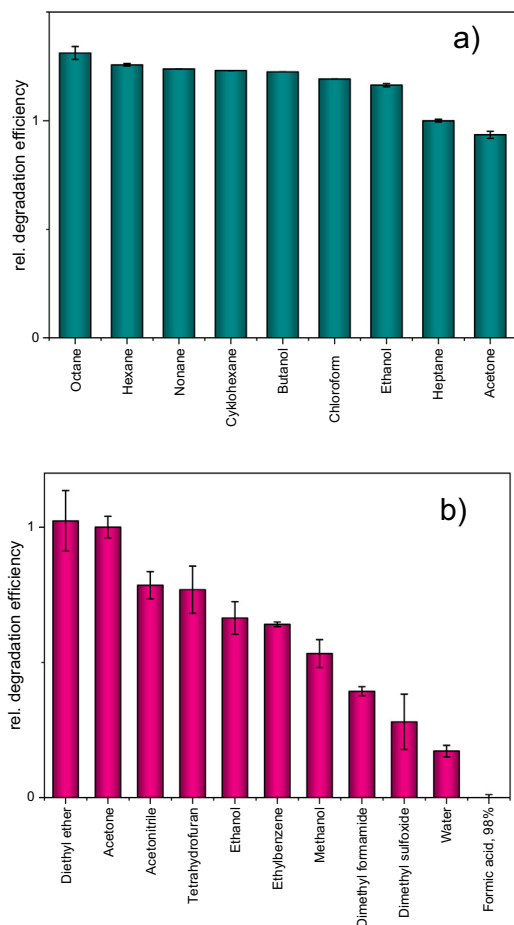


Fig. 6 (a) Relative degradation efficiency of the air-dried cerium oxide in various mixed solvents consisting of heptane and other co-solvent. Heptane to co-solvent ratio 1: 2. (b) Relative degradation efficiency of the air-dried cerium oxide in various mixed solvents consisting of acetonitrile and other co-solvent. Acetonitrile to co-solvent ratio 1: 2. (c) Correlation between the degradation efficiency of cerium oxide (rate constant) and the hydrogen bond donation (HBD) ability of co-solvents expressed as the $E_T(30)$ parameter. (d) Similar correlation of selected co-solvents between the rate constant and the α parameter. Both α and $E_T(30)$ were taken from Taft and Kamlet, 1979. (e) Correlation between the rate constant of parathion methyl degradation and the polarity parameter $E_T(30)$ of selected alcohols.

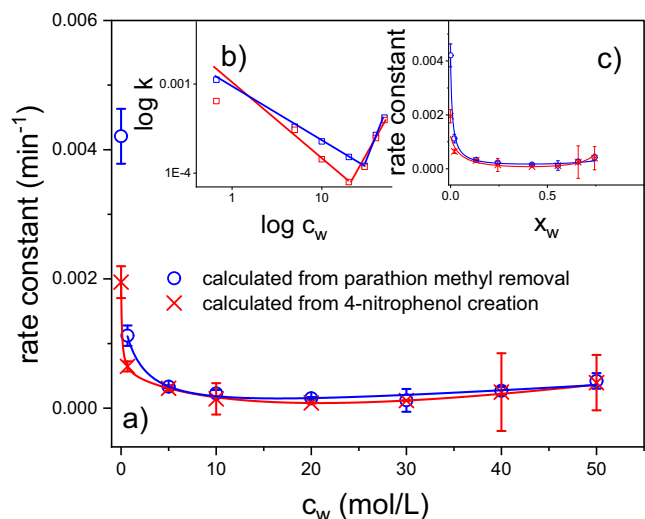


Fig. 7 (a) Degradation of parathion methyl in the presence of cerium oxide in the acetonitrile – H₂O mixture. Experimental conditions: The initial concentration of cerium oxide was 33 mg/mL, the initial concentration of parathion methyl was 1.33 mg/mL, and the equilibration time was 16 h. The degradation efficiency was expressed as a rate constant determined from the degree of conversion at a fixed time. The solid lines were fitted using an equation for the dependence of the hydrogen bond donating (HBD) ability of the acetonitrile – water binary solutions. (b) The same dependence was subdivided into the contributions of specific interactions (1) and electrostatic interactions (2); the red squares = experimental data for parathion methyl degradation.

$$= [S](1 + K_A[A]) + K_W[W] + [A] \sum_{i=1}^n K_i[W]^i \quad (8)$$

where $K_i = K_{C_i}K_{S_i}$. As the concentrations of active sites are typically low in comparison with the concentrations of solvents, the concentrations $[A]$ and $[W]$ may be approximated with c_A and c_W , respectively.

It is further assumed that various solvation species summarized in Eq. (8) contribute to the overall (observed) rate constant according to the following equation:

$$k_{obs} = \sum k_j F_j \quad (9)$$

where F_j are the fractions of the respective species (e.g., $F_{SAWi} = [SAW_i]/c_S$) and k_j are the constants specific for the respective species. When Eqs. (5) and (6) are combined, we obtain.

$$k_{obs} = \frac{k_0 + k_A K_A c_A + k_W K_W c_W + c_A \sum_{i=1}^n k_i K_i c_W^i}{1 + K_A c_A + K_W c_W + c_A \sum_{i=1}^n K_i c_W^i} \quad (10)$$

Eq. (10) relates the degradation efficiency of cerium oxide to the composition of the acetonitrile–water mixture; k_i reflects the fact that various microheterogeneities or various arrangements of the acetonitrile–water clusters may be more or less effective in the solvation of the binding site on the cerium oxide surface. This idea is also quite compatible with the presumption that a specific spatial arrangement of the Ce³⁺/Ce⁴⁺ pairs and –OH groups is required to create the active site.

It was found that Eq. (10) gives a reasonable fit to the experimental data for $n = 3$. However, k_i and other parameters in Eq. (10) are not accessible experimentally and are not found in the literature. Therefore, we tried to relate the degradation efficiency to other parameters commonly used to compare the behaviour of solvents or their mixtures. The most frequently used parameter is the Dimroth-Richardt empirical parameter $E_T(30)$, which corresponds to the excitation energy of the solvatochromic indicator (2,6-diphenyl-4-(2,4,6-triphenylpyridin-1-ium)-1-phenolate, also known as $E_T(30)$ dye) in various solvents, which is usually considered a measure of polarity, and it was successfully related to various thermodynamic and kinetic properties not only in single-component solvents but also in solvent mixtures (Skwierzynski and Connors, 1994; Bosch and Rosés, 1992).

An extensive comparison was published by Roses et al. (1995); who used the solvent-exchange model to derive equations for the $E_T(30)$ parameter in binary mixtures. In their work, an alternative approach based on preferential solvation was also described. For the water-acetonitrile mixture, the equation was derived in the following form (E_T is used instead of $E_T(30)$ for simplicity):

$$E_T = E_{T1} + \frac{a(x_2^0)^2 + c(1 - x_2^0)x_2^0}{(1 - x_2^0)^2 + f_{2/1}(x_2^0)^2 + f_{12/1}(1 - x_2^0)x_2^0} \quad (11)$$

where.

$$a = f_{2/1}(E_{T2} - E_{T1}) \quad (12)$$

and.

$$c = f_{12/1}(E_{T12} - E_{T1}) \quad (13)$$

is the mole fraction of the more polar solvent (water) in the binary mixture. E_{T1} and E_{T2} are values of the $E_T(30)$ parameter for pure solvents (acetonitrile, water), whereas E_{T12} corresponds to the (hypothetical) mixed solvent, and $f_{2/1}$ and $f_{12/1}$ are parameters of preferential solvation. Numerical values of these parameters for several solvent mixtures are listed in the aforementioned paper (Rosés et al., 1995); including those of acetonitrile and water. Using these parameters, Eq. (8) gives a relatively simple monotonous curve that can be transformed to the curve expressing the experimental dependence of degradation efficiency on the composition of the solvent mixture. Nevertheless, this equation can be used to fit the experimental data on the condition that E_T and f are treated as adjustable parameters (see Fig. 7c).

The experimental dependence in Fig. 7 reflects the inherently complex nature of mixtures consisting of organic solvents and water (Salmar et al., 2012; Saleh et al., 2006). The dependence of the reaction rate on the water content may be divided into two (or even more) regions, in which various interactions predominate. In the water-rich region, nonspecific (mainly electrostatic) interactions predominate, which was also confirmed by the linear dependence between the logarithm of the rate constant and the reciprocal value of the dielectric constant (Fig. 8). In the acetonitrile-rich region, however, solvent–solute interactions play an important role. The addition of even small amounts of water into the reaction mixture causes preferential solvation of the active sites accompanied by a dramatic decrease in the degradation efficiency. An almost identical dependence was found for the reaction of sodium 4-nitrophenoxide with iodomethane in the acetone–water mix-

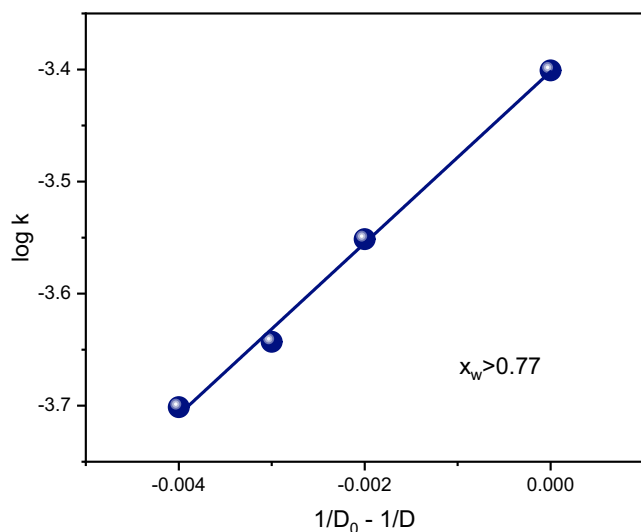


Fig. 8 Dependence of the rate constant on the dielectric constant in the acetonitrile–water mixture for the water-rich region (compare with the similar dependence for the acetone–water mixture in Eduardo Humeres, 2001).

ture; this reaction presumably proceeded by the S_N2 mechanism (Eduardo Humeres, 2001).

4. Conclusions

It was shown that surface hydroxyls play a crucial role in the destruction of the molecules of toxic organophosphates in the presence of cerium oxide. However, the $-OH$ groups are consumed during phosphoester destruction, and thus, the respective materials should be considered stoichiometric sorbents (reagents) (Klabunde et al., 1996) rather than catalysts.

Parathion methyl degradation proceeds well in nonpolar solvents as well as in aprotic solvents. In solvents with hydrogen bond donating ability, however, the $-OH$ groups on the cerium oxide surface are solvated and inactivated. As shown for the acetonitrile–water reaction mixture, the addition of even small amounts of protic solvent, such as water, dramatically deteriorates the cerium oxide degradation efficiency. The model of preferential solvation was used to express the experimental dependencies of the cerium oxide degradation efficiency on the mixture composition in the whole concentration range. In certain solvent systems, some empirical polarity scales, such as the alpha-scale or the Dimroth-Richardt parameter $E_T(30)$, may be correlated with the degradation efficiency of cerium oxide.

Declaration of Competing Interest

The authors declare that they have no known competing financial interests or personal relationships that could have appeared to influence the work reported in this paper.

Acknowledgements

The authors acknowledge the assistance provided by the Research Infrastructure NanoEnviCz, supported by the Ministry of Education, Youth and Sports of the Czech Republic under Project No. LM2018124 and Czech Scientific Foundation (grant No. 19-07460S).

The authors have no conflicts of interest to declare.

References

- K.J. Klabunde, J. Stark, O. Koper, C. Mohs, D.G. Park, S. Decker, Y. Jiang, I. Lagadic, D. Zhang, Nanocrystals as stoichiometric reagents with unique surface chemistry, *J. Phys. Chem.* 100 (1996) 12142–12153. <http://www.scopus.com/inward/record.url?eid=2-s2.0-0030198228&partnerID=tZOtx3y1>.
- Khaleel, A., Li, W., Klabunde, K.J., 1999. Nanocrystals as stoichiometric reagents with unique surface chemistry, New adsorbents for air purification. *Nanostructured Mater.* 12, 463–466. [https://doi.org/10.1016/S0965-9773\(99\)00159-2](https://doi.org/10.1016/S0965-9773(99)00159-2).
- Rajagopalan, S., Koper, O., Decker, S., Klabunde, K.J., 2002. Nanocrystalline Metal Oxides as Destructive Adsorbents for Organophosphorus Compounds at Ambient Temperatures. *Chem. - A Eur. J.* 8, 2602. [https://doi.org/10.1002/1521-3765\(20020603\)8:11<2602::AID-CHEM2602>3.0.CO;2-3](https://doi.org/10.1002/1521-3765(20020603)8:11<2602::AID-CHEM2602>3.0.CO;2-3).
- Lucas, E., Decker, S., Khaleel, A., Seitz, A., Fultz, S., Ponce, A., Li, W., Carnes, C., Klabunde, K.J., 2001. Nanocrystalline metal oxides as unique chemical reagents/sorbents. *Chemistry.* 7, 2505–2510. [https://doi.org/10.1002/1521-3765\(20010618\)7:12<2505::AID-CHEM25050>3.0.CO;2-R](https://doi.org/10.1002/1521-3765(20010618)7:12<2505::AID-CHEM25050>3.0.CO;2-R).
- Štengl, V., Henych, J., Janoš, P., Skoumal, M., 2016. Nanostructured Metal Oxides for Stoichiometric Degradation of Chemical Warfare Agents. *Rev. Environ. Contam. Toxicol.* 236, 239–258. https://doi.org/10.1007/978-3-319-20013-2_4.
- Houšková, V., Štengl, V., Bakardjieva, S., Murafa, N., Kalendová, A., Opluštil, F., 2007. Nanostructure materials for destruction of warfare agents and eco-toxins prepared by homogeneous hydrolysis with thioacetamide: Part I—zinc oxide. *J. Phys. Chem. Solids* 68, 716–720. <https://doi.org/10.1016/j.jpcs.2006.12.012>.
- Štengl, V., Králová, D., Opluštil, F., Němec, T., 2012. Mesoporous manganese oxide for warfare agents degradation. *Microporous Mesoporous Mater.* 156, 224–232. <https://doi.org/10.1016/j.micromeso.2012.02.031>.
- Janoš, P., Ederer, J., Došek, M., 2014. Some environmentally relevant reactions of cerium oxide. *Nov. Biotechnol. Chim.* 13. <https://doi.org/10.1515/nbec-2015-0005>.
- Ederer, J., Štastný, M., Došek, M., Henych, J., Janoš, P., 2019. Mesoporous cerium oxide for fast degradation of aryl organophosphate flame retardant triphenyl phosphate. *RSC Adv.* 9, 32058–32065. <https://doi.org/10.1039/c9ra06575j>.
- Denet, E., Betzabeth Espina-Benitez, M., Pitault, I., Pollet, T., Blaha, D., Bolzinger, M.-A., Rodriguez Nava, V., Briançon, S., 2020. Metal oxide nanoparticles for the decontamination of toxic chemical and biological compounds. *Int. J. Pharm.* 583. <https://doi.org/10.1016/j.ijpharm.2020.119373>.
- Janoš, P., Kuran, P., Kormunda, M., Štengl, V., Grygar, T.M., Dosek, M., Štastný, M., Ederer, J., Pilarova, V., Vrtoch, L., 2014. Cerium dioxide as a new reactive sorbent for fast degradation of parathion methyl and some other organophosphates. *J. Rare Earths* 32, 360–370. [https://doi.org/10.1016/S1002-0721\(14\)60079-X](https://doi.org/10.1016/S1002-0721(14)60079-X).
- N.S. Gould, S. Li, H.J. Cho, H. Landfield, S. Caratzoulas, D. Vlachos, P. Bai, B. Xu, Understanding solvent effects on adsorption and protonation in porous catalysts, *Nat. Commun.* 2020 11.11 (2020) 1–13. <https://doi.org/10.1038/s41467-020-14860-6>.
- Janoš, P., Ederer, J., Došek, M., Štojdl, J., Henych, J., Tolasz, J., Kormunda, M., Mazanec, K., 2019. Can cerium oxide serve as a phosphodiesterase-mimetic nanozyme? *Environ. Sci. NANO* 6, 3684–3698. <https://doi.org/10.1039/C9EN00815B>.
- Tolasz, J., Henych, J., Štastný, M., Němečková, Z., Slušná, M.Š., Opletal, T., Janoš, P., 2020. Room-temperature synthesis of nanoceria for degradation of organophosphate pesticides and its regeneration and reuse. *RSC Adv.* 10, 14441–14450. <https://doi.org/10.1039/d0ra00937g>.
- Ederer, J., Janoš, P., Štastný, M., Henych, J., Ederer, K., Slušná, M.Š., Tolasz, J., 2021. Nanocrystalline cerium oxide for catalytic degradation of paraoxon methyl: Influence of CeO₂ surface

- properties. *J. Environ. Chem. Eng.* 9. <https://doi.org/10.1016/J.JECE.2021.106229> 106229.
- Johnson, M.F.L., Mooi, J., 1987. Cerium dioxide crystallite sizes by temperature-programmed reduction. *J. Catal.* 103, 502–505. [https://doi.org/10.1016/0021-9517\(87\)90142-4](https://doi.org/10.1016/0021-9517(87)90142-4).
- P. Janoš, M. Petrák, Preparation of ceria-based polishing powders from carbonates, *J. Mater. Sci.* 1991 2615. 26 (1991) 4062–4066. <https://doi.org/10.1007/BF02402947>.
- Ederer, J., Janoš, P., Ecorchard, P., Tolasz, J., Štengl, V., Beneš, H., Perchacz, M., Pop-Georgievski, O., 2017. Determination of amino groups on functionalized graphene oxide for polyurethane nanomaterials: XPS quantitation vs. functional speciation. *RSC Adv.* 7, 12464–12473. <https://doi.org/10.1039/C6RA28745J>.
- STANAG 4653, 2012. *Combined Operational Characteristics, Technical specifications, Test Procedures and Evaluation Criteria for Chemical, Biological, Radiological Nuclear Decontamination Equipment.*
- Seal, S., Jeyaranjan, A., Neal, C.J., Kumar, U., Sakthivel, T.S., Sayle, D.C., 2020. Engineered defects in cerium oxides: Tuning chemical reactivity for biomedical, environmental, & energy applications. *Nanoscale* 12, 6879–6899. <https://doi.org/10.1039/d0nr01203c>.
- Plakhova, T.V., Romanchuk, A.Y., Butorin, S.M., Konyukhova, A. D., Egorov, A.V., Shiryaev, A.A., Baranchikov, A.E., Dorovotovskii, P.V., Huthwelker, T., Gerber, E., Bauters, S., Sozarukova, M.M., Scheinost, A.C., Ivanov, V.K., Kalmykov, S.N., Kvashnina, K.O., 2019. Towards the surface hydroxyl species in CeO₂ nanoparticles. *Nanoscale*. 11, 18142–18149. <https://doi.org/10.1039/c9nr06032d>.
- Artiglia, L., Van Bokhoven, J.A., Ghosalya, M.K., Li, X., Beck, A., 2021. Size of Ceria Particles Influences Surface Hydroxylation and Hydroxyl Stability. *J. Phys. Chem. C* 125, 9303–9309. <https://doi.org/10.1021/ACS.JPC.1C01718>.
- Hamlin, T.A., Swart, M., Bickelhaupt, F.M., Vch, W., 2018. Nucleophilic Substitution (S_N2): Dependence on Nucleophile, Leaving Group, Central Atom, Substituents, and Solvent. *ChemPhysChem* 19, 1315–1330. <https://doi.org/10.1002/cphc.201701363>.
- Taft, R.W., Kamlet, M.J., 1979. Linear solvation energy relationships. Part 4. Correlations with and limitations of the α scale of solvent hydrogen bond donor acidities. *J. Chem. Soc. Perkin Trans. 2*, 1723–1729. <https://doi.org/10.1039/P29790001723>.
- Marcus, Y., 1991. The effectiveness of solvents as hydrogen bond donors. *J. Solution Chem.* 20, 929–944. <https://doi.org/10.1007/BF01074953>.
- Takamuku, T., Tabata, M., Yamaguchi, A., Nishimoto, J., Kumamoto, M., Wakita, H., Yamaguchi, T., 1998. Liquid structure of acetonitrile-water mixtures by X-ray diffraction and infrared spectroscopy. *J. Phys. Chem. B* 102, 8880–8888. <https://doi.org/10.1021/jp9824297>.
- Nagasaka, M., Yuzawa, H., Kosugi, N., 2020. Microheterogeneity in Aqueous Acetonitrile Solution Probed by Soft X-ray Absorption Spectroscopy. *J. Phys. Chem. B* 124, 1259–1265. <https://doi.org/10.1021/ACS.JPCB.0C00551>.
- Ahn, D.S., Lee, S., 2007. Density Functional Theory Study of Acetonitrile-Water Clusters: Structures and Infrared Frequency Shifts. *Bull. Korean Chem. Soc.* 28, 725–729. <https://doi.org/10.5012/bkcs.2007.28.5.725>.
- Skwierzynski, R.D., Connors, K.A., 1994. Solvent effects on chemical processes. Part 7. Quantitative description of the composition dependence of the solvent polarity measure ET(30) in binary aqueous-organic solvent mixtures. *J. Chem. Soc. Perkin Trans. 2*, 467–472. <https://doi.org/10.1039/p29940000467>.
- Bosch, E., Rosés, M., 1992. Relationship between ET polarity and composition in binary solvent mixtures. *J. Chem. Soc., Faraday Trans. 88*, 3541–3546. <https://doi.org/10.1039/FT9928803541>.
- Rosés, M., Ráfols, C., Ortega, J., Bosch, E., 1995. Solute-solvent and solvent-solvent interactions in binary solvent mixtures. Part 1. A comparison of several preferential solvation models for describing ET(30) polarity of dipolar hydrogen bond acceptor-cosolvent mixtures. *J. Chem. Soc. Perkin Trans. 2*, 1607–1615. <https://doi.org/10.1039/p29950001607>.
- Salmar, S., Järv, J., Tenno, T., Tuulmets, A., 2012. Role of water in determining organic reactivity in aqueous binary solvents. *Cent. Eur. J. Chem.* 10, 1600–1608. <https://doi.org/10.2478/s11532-012-0080-8>.
- Saleh, M.A., Akhtar, S., Ahmed, M.S., 2006. Density, viscosity and thermodynamic activation of viscous flow of water + acetonitrile. *Phys. Chem. Liq.* 44, 551–562. <https://doi.org/10.1080/00319100600861151>.
- *,† Eduardo Humeres, † Ricardo J. Nunes, ‡ Vanderlei G. Machado, § and Marcelo D. G. Gasques, C. Machado§, Ion-Dipole S_N2 Reaction in Acetone–Water Mixtures. *Electrostatic and Specific Solute–Solvent Interactions*, (2001). <https://doi.org/10.1021/JO0012501>.